

Obliquity Constraints for the Extremely Eccentric Sub-Saturn Kepler-1656 b

RYAN A. RUBENZAHL,^{1,*} ANDREW W. HOWARD,¹ SAMUEL HALVERSON,² CRISTOBAL PETROVICH,^{3,4} ISABEL ANGELO,⁵
GUÐMUNDUR STEFÁNSSON,⁶ FEI DAI,⁷ AARON HOUSEHOLDER,^{8,9} BENJAMIN FULTON,¹⁰ STEVEN R. GIBSON,¹¹
ARPITA ROY,¹² ABBY P. SHAUM,¹ HOWARD ISAACSON,¹³ MAX BRODHEIM,¹⁴ WILLIAM DEICH,¹⁵ GRANT M. HILL,¹⁴
BRADFORD HOLDEN,¹⁵ DANIEL HUBER,^{7,16} RUSS R. LAHER,¹⁰ KYLE LANCIOS,¹⁴ JOEL N. PAYNE,¹⁴
ERIK A. PETIGURA,⁵ CHRISTIAN SCHWAB,¹⁷ JOSH WALAWENDER,¹⁴ SHARON X. WANG,¹⁸ LAUREN M. WEISS,¹⁹
JOSHUA N. WINN,²⁰ AND JASON T. WRIGHT^{21,22,23}

¹*Department of Astronomy, California Institute of Technology, Pasadena, CA 91125, USA*

²*Jet Propulsion Laboratory, California Institute of Technology, 4800 Oak Grove Drive, Pasadena, CA 91109*

³*Department of Astronomy, Indiana University, 727 East 3rd Street, Bloomington, IN 47405-7105, USA*

⁴*Millennium Institute for Astrophysics, Santiago, Chile*

⁵*Department of Physics & Astronomy, University of California Los Angeles, Los Angeles, CA 90095, USA*

⁶*Anton Pannekoek Institute for Astronomy, University of Amsterdam, Science Park 904, 1098 XH Amsterdam, The Netherlands*

⁷*Institute for Astronomy, University of Hawai'i, 2680 Woodlawn Drive, Honolulu, HI 96822, USA*

⁸*Department of Earth, Atmospheric and Planetary Sciences, Massachusetts Institute of Technology, Cambridge, MA 02139, USA*

⁹*Kavli Institute for Astrophysics and Space Research, Massachusetts Institute of Technology, Cambridge, MA 02139, USA*

¹⁰*NASA Exoplanet Science Institute/Caltech-IPAC, MC 314-6, 1200 E. California Blvd., Pasadena, CA 91125, USA*

¹¹*Caltech Optical Observatories, Pasadena, CA, 91125, USA*

¹²*Astrophysics & Space Institute, Schmidt Sciences, New York, NY 10011, USA*

¹³*501 Campbell Hall, University of California at Berkeley, Berkeley, CA 94720, USA*

¹⁴*W. M. Keck Observatory, Waimea, HI 96743, USA*

¹⁵*UC Observatories, University of California, Santa Cruz, CA 95064, USA*

¹⁶*Sydney Institute for Astronomy (SIfA), School of Physics, University of Sydney, NSW 2006, Australia*

¹⁷*School of Mathematical and Physical Sciences, Macquarie University, Balaclava Road, North Ryde, NSW 2109, Australia*

¹⁸*Department of Astronomy, Tsinghua University, Beijing 100084, People's Republic of China*

¹⁹*Department of Physics and Astronomy, University of Notre Dame, Notre Dame, IN 46556, USA*

²⁰*Department of Astrophysical Sciences, Princeton University, Princeton, NJ 08544, USA*

²¹*Department of Astronomy & Astrophysics, 525 Davey Laboratory, Penn State, University Park, PA, 16802, USA*

²²*Center for Exoplanets and Habitable Worlds, 525 Davey Laboratory, Penn State, University Park, PA, 16802, USA*

²³*Penn State Extraterrestrial Intelligence Center, 525 Davey Laboratory, Penn State, University Park, PA, 16802, USA*

ABSTRACT

The orbits of close-in exoplanets provide clues to their formation and evolutionary history. Many close-in exoplanets likely formed far out in their protoplanetary disks and migrated to their current orbits, perhaps via high-eccentricity migration (HEM), a process that can also excite obliquities. A handful of known exoplanets are perhaps caught in the act of HEM, as they are observed on highly eccentric orbits with tidal circularization timescales shorter than their ages. One such exoplanet is Kepler-1656 b, which is also the only known non-giant exoplanet ($<100 M_{\oplus}$) with an extreme eccentricity ($e = 0.84$). We measured the sky-projected obliquity of Kepler-1656 b by observing the Rossiter-McLaughlin effect during a transit with the Keck Planet Finder. Our data are consistent with an aligned orbit, but are also consistent with moderate misalignment with $\lambda < 50$ deg at 95% confidence, with the most likely solution of $35.0^{+14.9}_{-21.6}$ deg. A low obliquity would be an unlikely outcome of most eccentricity-exciting scenarios, but we show that the properties of the outer companion in the system are consistent with the coplanar HEM mechanism. Alternatively, if the system is not relatively coplanar ($\lesssim 20$ deg mutual inclination), Kepler-1656 b may be presently at a rare snapshot of long-lived eccentricity oscillations that do not induce migration. Kepler-1656 b is only the fourth exoplanet with $e > 0.8$ to have its obliquity constrained; expanding this population will help establish the degree to which orbital misalignment accompanies migration. Future work that constrains the mutual inclinations of outer perturbers will be key for distinguishing plausible mechanisms.

1. INTRODUCTION

High-eccentricity migration (HEM) is a leading explanation for the formation of close-in giant exoplanets, such as hot Jupiters (HJs), with orbital periods less than 10 days (Dawson & Johnson 2018; Rice et al. 2022). In the HEM scenario, the giant planet forms beyond a few AU and is excited to extremely high eccentricity ($e > 0.9$) either through planet-planet scattering (Rasio & Ford 1996, e.g.) or secular interactions with an outer planetary or stellar companion (Fabrycky & Tremaine 2007; Naoz et al. 2011; Teyssandier et al. 2013). To excite large enough eccentricities, the companion must either possess a large mutual inclination to the inner planet, in which case von-Zeipel Kozai-Lidov (ZKL; Kozai 1962; Lidov 1962; Ito & Ohtsuka 2019) oscillations can occur, or the companion must have an eccentric orbit, in which case higher-order eccentric Kozai-Lidov (EKL; Naoz et al. 2013; Naoz et al. 2013; Naoz 2016) oscillations can yield the same result. Subsequently, tidal interactions with the star at periastron passage (e.g., Rasio & Ford 1996; Wu 2018) circularize the orbit, causing the planet to migrate. These eccentricity-exciting mechanisms can also excite a broad range of stellar obliquities (see Albrecht et al. 2022a for a review), the angle between the host star’s rotation axis and the normal to the exoplanet’s orbital plane. Obliquity damping mechanisms may then come into play, as we observe HJs to be aligned around cool stars (below the Kraft Break, $\lesssim 6250$ K; Kraft 1967) and misaligned around hot stars (Winn et al. 2010; Schlaufman 2010). Cool stars are able to damp HJ obliquities faster than the age of the system either through tidal effects in their convective envelopes (Albrecht et al. 2012; Lai 2012; Dawson 2014) or resonance locking in their radiative cores (Zanazzi et al. 2024).

There is no reason, however, that HEM should be limited to giant planets. Many small ($< 100 M_{\oplus}$) close-in exoplanets likely migrated from further out in their protoplanetary disks, as evidenced by their large envelope mass fraction (e.g., WASP-107 b, Piaulet et al. 2021) and/or highly inclined orbit (Albrecht et al. 2022a; Atia et al. 2023). Misaligned orbits could arise from the HEM process or be excited post-formation through interactions such as resonance crossing during the disk-dispersal stage (Petrovich et al. 2020) or nodal precession cycles (Yee et al. 2018; Rubenzahl et al. 2021), in either case with the same outer companion that triggered HEM. Though, the census of outer companions to

close-in small planets with measured obliquities is relatively incomplete. Only HAT-P-11 (Yee et al. 2018) and WASP-107 (Piaulet et al. 2021) have fully-resolved outer companions. While these mechanisms require a large mutual inclination between the inner and outer planet, only HAT-P-11 has a mutual inclination measurement (near polar; Xuan & Wyatt 2020).

If exoplanets do experience HEM, then we should expect to observe a few systems in the act of migration (Socrates et al. 2012). Approximately half a dozen known exoplanets have an eccentricity and semimajor axis such that the tidal circularization timescale is less than the age of the system (so the planet’s orbit should still be circularizing), and such that the planet is not expected to be engulfed by its host star; see Figure 1. Several of these have obliquity measurements. Most recently, the proto-HJ TOI-3362 b (Dong et al. 2021) was found to be aligned to within 3 deg (Espinoza-Retamal et al. 2023). This striking result indicates that perhaps some planets are able to migrate without obtaining a large obliquity. Petrovich (2015a) found that coplanar HEM (CHEM) can occur as a result of EKL oscillations between an outer planetary perturber (“c”) and the inner proto-HJ (“b”), provided the outer planet be relatively eccentric ($e_c > 0.67$ if $e_b = 0$ or both $e_b, e_c > 0.5$) and the planets maintain a low mutual inclination (< 20 deg). However, any outer planetary companions in the TOI-3362 system remain undetected.

Kepler-1656 b is another such highly eccentric exoplanet ($e_b = 0.84 \pm 0.01$, $48 M_{\oplus}$, 31 day; Brady et al. 2018), and is the only known member of this class less massive than $100 M_{\oplus}$. Kepler-1656 b is also the only highly eccentric exoplanet with a known outer planetary companion. Angelo et al. (2022) discovered Kepler-1656 c ($M_c \sin i_{\text{orb},c} = 0.4 \pm 0.1 M_J$), a giant planet in a wide (~ 2000 day) and eccentric ($e_c = 0.53 \pm 0.05$) orbit. These authors ran a suite of dynamical integrations using the EKL formalism (Naoz 2016) and found that those which matched the observed system properties either rapidly ($\lesssim 1$ Gyr) circularized into a HJ-like orbit (or in a few cases crashed into the star), or achieved high eccentricity through EKL oscillations which could persist much longer than the age of the system (6.3 Gyr) without inducing tidal migration. These solutions tended to occur at high (60deg–130deg) mutual inclinations and would often ($\gtrsim 75\%$) excite planet b to large stellar obliquities (> 40 deg).

In this letter, we report our measurement of the stellar obliquity of Kepler-1656 b. We present our observations of a single transit of Kepler-1656 b with the Keck Planet Finder in Section 2.1. In Section 2.2 we

* NSF Graduate Research Fellow

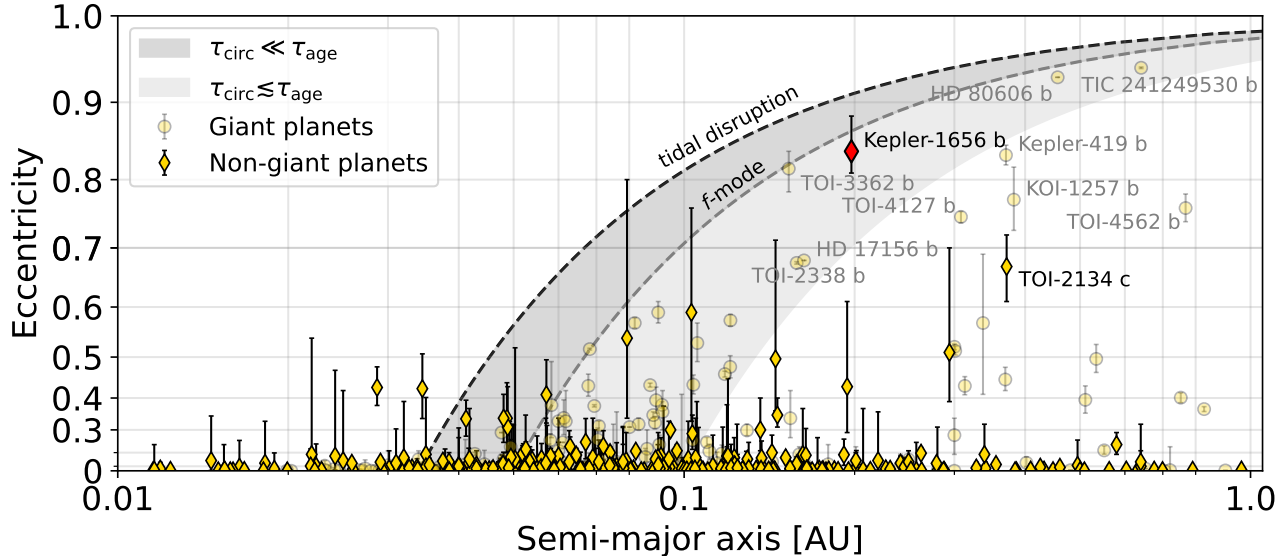


Figure 1. Eccentricity-semimajor axis diagram for transiting exoplanets. Giant planets, defined as $>100 M_{\oplus}$ or $>8 R_{\oplus}$ if there is no mass measurement, are plotted as faded points. Following Dong et al. (2021), the y-axis is scaled uniformly in e^2 , and the high-eccentricity migration track is shaded in light grey. The dashed grey line traces $a = 0.05/(1 - e^2)$, corresponding to the minimum semimajor axis to excite f-mode oscillations and produce rapid orbital decay (Wu 2018). Planets above this line would therefore be extremely rare. The black dashed upper boundary ($0.034/(1 - e^2)$) represents the line of constant angular momentum where a $1 M_J$, $1.3 R_J$ exoplanet would become tidally disrupted at its closest approach to a solar mass star (Dong et al. 2021); no giant planets can persist above this boundary. The lower boundary ($0.1/(1 - e^2)$) corresponds to a final semimajor axis of 0.1 AU, beyond which circularization timescales become much longer than typical system ages. The boundaries are not exact as they depend on the strength and efficiency of tides in the system. Exoplanets with $e > 0.6$ are labelled; Kepler-1656 b is the only sub-Saturn firmly in the HEM track. Data are from the NASA Exoplanet Archive, accessed on 2024-04-01 (NASA Exoplanet Archive 2019).

modeled the Rossiter-McLaughlin (RM; Rossiter 1924; McLaughlin 1924) effect in our transit radial velocity time series and derived a projected stellar obliquity of $|\lambda| = 35.0^{+14.9}_{-21.6}$ deg, though the data are fully consistent with an aligned orbit. We discuss the implications of this result on the dynamical history of the system and place Kepler-1656 b in the context of the broader exoplanet population in Section 3, and conclude in Section 4.

2. OBLIQUITY MEASUREMENT

2.1. Observations

We observed a single transit of Kepler-1656 b on UT June 30, 2023 with the Keck Planet Finder (KPF; Gibson et al. 2016, 2018, 2020). We used a fixed exposure time of 480 sec to average over solar-type oscillations (Brown et al. 1991; Chaplin et al. 2019) and reach a typical signal-to-noise ratio (S/N) of 100. We used the public KPF data reduction pipeline (DRP)¹ to derive cross-correlation functions (CCFs; Baranne et al. 1996) using the G2 ESPRESSO weighted binary mask (Pepe

et al. 2002). Orders with heavy telluric contamination are thus automatically not included in the analysis. We obtained the radial velocity (RV) as the centroid of a fitted Gaussian to the CCF. We separately extracted an RV from the green and red channels of KPF and combined the two in a weighted average, taking the weight to be proportional to the relative flux in each channel and constant in time. The resulting RV time series (shown in Figure 2) spans a baseline from 1 hr before to 1 hr after the transit.

2.2. Rossiter-McLaughlin Modeling

We fit the RV time series using *rmfit* (Stefánsson et al. 2022), a Python-based model for the anomalous RV produced by the RM effect based on the equations of Hirano et al. (2011). We adopted the ephemeris from Brady et al. (2018) based on their fits to the *Kepler* transit light curves and adopted their fitted values as Gaussian priors for the time of conjunction (t_c), orbital period (P_{orb}), transit depth (R_p/R_*), scaled semimajor axis (a/R_*), orbital inclination (i_{orb}), orbital eccentricity (e), and argument of periastron (ω). Limb darkening coefficients for the KPF bandpass (V) were computed with EXOFAST (Eastman et al. 2013), incorporating the

¹ <https://github.com/Keck-DataReductionPipelines/KPF-Pipeline/>

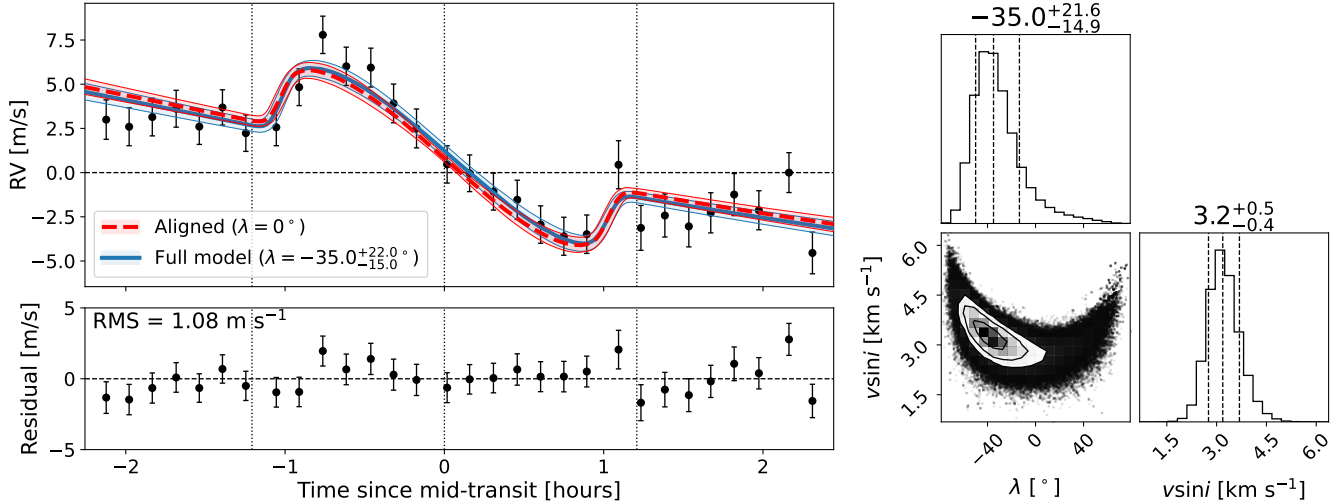


Figure 2. **Left:** The KPF RV time series, in black, during the transit of Kepler-1656 b. The blue curve shows the median RV from the posterior distribution of the full model, with the shaded band denoting the 16th–84th percentiles. The red curve shows the same for the aligned model where λ is fixed to 0 deg. The bottom panel shows the residuals to the median full model. **Right:** The posterior distribution for λ and $v \sin i_*$ for the full model. Misaligned λ requires $v \sin i_* > 3 \text{ km s}^{-1}$.

spectroscopic T_{eff} ($5731 \pm 60 \text{ K}$), $[\text{Fe}/\text{H}]$ (0.19 ± 0.04), and $\log(g)$ (4.37 ± 0.10) from Brady et al. (2018).

There are two existing literature measurements of $v \sin i_*$ for Kepler-1656. The California-Kepler Survey (Petigura et al. 2017) reported a value of $2.8 \pm 1.0 \text{ km s}^{-1}$ from a SpecMatch-Synthetic (Petigura 2015) analysis of a Keck/HIRES spectrum. We reanalyzed the same HIRES spectrum with SpecMatch-Synthetic and instead obtained an upper bound of $< 2 \text{ km s}^{-1}$, which SpecMatch-Synthetic reports if the spectrum is dominated by instrument broadening. However, Masuda et al. (2022) found while analyzing > 100 Keck/HIRES FG-type spectra that the population-level distributions obtained by applying SpecMatch-Synthetic to their sample were more consistent if upper-limits were instead interpreted as $< 3 \text{ km s}^{-1}$. Kepler-1656 also appeared in the catalog of Brewer et al. (2016), who found a smaller $v \sin i_*$ of 1.1 km s^{-1} with 3.2 km s^{-1} macroturbulence, though this is also likely limited by instrumental broadening. As a result, we opted to place a Gaussian prior on $v \sin i_*$ of $2.8 \pm 1.0 \text{ km s}^{-1}$ from the CKS result and not restrict $v \sin i_*$ to any upper-bound.

The main free parameter in our model is the sky-projected obliquity, λ . The parameter quantifying the non-rotational line broadening, v_β , was unconstrained by the RM data, so we fixed this value to 3 km s^{-1} based on a 2.6 km s^{-1} (FWHM) instrumental broadening from KPF and the intrinsic line dispersion for $T_{\text{eff}} = 5731 \text{ K}$ from Eq. (20) in (Hirano et al. 2011). Our model is a combination of a Keplerian RV signal and the RM effect, with an arbitrary offset term (γ). For the Keplerian term, we adopted the best-fit K_b from Angelo et al.

(2022) as a prior. Because of the low amplitude of the RM signal ($\sim 4.5 \text{ m s}^{-1}$), we also included the convective blueshift effect parameterized by v_{CB} using the prescription of Shporer & Brown (2011), which can contribute at the m s^{-1} level. We set a wide prior of $\pm 10 \text{ km s}^{-1}$ on v_{CB} . Lastly, we include a RV jitter term (σ_{jit}) to account for any underestimated white noise.

We first found the maximum a-posteriori (MAP) solution using the PyDE differential evolution optimizer (Parviainen 2016). This solution was used as a starting point for a Markov-Chain Monte Carlo (MCMC) exploration of the posterior. We ran an EnsembleSampler with 100 walkers using the package emcee (Foreman-Mackey et al. 2013), each of which obtained 30,000 samples. We discarded the first 10% as “burn-in” and checked for convergence by requiring the Gelman–Rubin statistic (Gelman et al. 2003) be $\ll 1\%$ of unity for all parameters and ensuring that the autocorrelation time was $< 2\%$ the length of the independent chains per walker (Hogg & Foreman-Mackey 2018). The posteriors in λ and $v \sin i_*$ were unaffected by the inclusion of v_{CB} , which itself is orthogonal to the RM effect and was not detected ($v_{CB} = -560 \pm 930 \text{ km s}^{-1}$). As a result, we fixed $v_{CB} = 0 \text{ km s}^{-1}$ in our final fit.

Our best-fitting RM model, shown in Figure 2, has $|\lambda| = 35.0_{-21.6}^{+14.9}$ deg. The negative λ solutions, which the MCMC exploration finds, correspond to $i_{\text{orb}} < 90$ deg. However, a symmetric positive solution for λ exists for $i_{\text{orb}} > 90$ deg. There is also a degeneracy between λ and $v \sin i_*$ due to the central (low impact parameter) transit. The RM fit found $v \sin i_* = 3.2_{-0.4}^{+0.5} \text{ km s}^{-1}$, which is consistent with the results from spectral broadening

but is also degenerate with varying λ (see Figure 2, right panel). The spectral fitting results downweight RM solutions with $v \sin i_*$ significantly greater than 3 km s^{-1} , i.e., larger values of λ . The full set of fitted parameters is tabulated in Table 1.

For comparison, we also fit a model with λ fixed to 0 deg. This aligned model, also shown in Figure 2, produces a fit with statistically indistinguishable goodness-of-fit metrics (χ^2 , BIC), though with a slightly larger σ_{jit} term (see Table 1). The aligned model yielded a lower $v \sin i_* = 2.7 \pm 0.3 \text{ km s}^{-1}$, which is slightly more consistent with the spectroscopic constraints. To summarize, neither an aligned model nor one with modest misalignment is ruled out by the data. Without any further information on $v \sin i_*$, our RM measurement can only constrain $|\lambda| < 57 \text{ deg}$ at 95% confidence.

Table 1. Best-fit RM Parameters

Parameter	Full model	Aligned model	Unit
$ \lambda $	$35.0^{+14.9}_{-21.6}$	0	$^\circ$
$v \sin i_*$	$3.2^{+0.5}_{-0.4}$	$2.7^{+0.3}_{-0.3}$	m s^{-1}
i_{orb}	$88.9^{+0.5}_{-0.5}$	$89.2^{+0.6}_{-0.6}$	$^\circ$
e	$0.824^{+0.013}_{-0.014}$	$0.824^{+0.013}_{-0.014}$	
ω	$54.5^{+4.7}_{-4.7}$	$54.7^{+4.8}_{-4.7}$	$^\circ$
K	$13.3^{+1.6}_{-1.5}$	$13.4^{+1.7}_{-1.6}$	m s^{-1}
γ	$-5.8^{+1.1}_{-1.1}$	$-5.5^{+1.1}_{-1.2}$	m s^{-1}
σ_{jit}	$0.51^{+0.37}_{-0.33}$	$0.7^{+0.34}_{-0.36}$	m s^{-1}
ΔBIC	0.0	5.0	
χ^2	0.92	0.95	

Posterior values display the 50th percentile with the upper and lower errorbars giving the difference relative to the 84th and 16th percentiles, respectively. The reduced χ^2 includes the median σ_{jit} added in quadrature to the measurement uncertainties.

Of note is the *Kepler* photometry of Kepler-1656, shown in Figure 3, which exhibits significant quasiperiodic variability. An autocorrelation analysis using *spinspotter* (Holcomb et al. 2022) detects a primary periodicity of 11.6 ± 0.9 days. If this signal corresponds to rotationally modulated starspots, then the stellar equatorial rotation speed is $4.7 \pm 1 \text{ km s}^{-1}$. Combining this value with our constraints on $v \sin i_*$ from the RM fit using the methodology of Masuda & Winn (2020), the corresponding stellar inclination is $47 \pm 28 \text{ deg}$. Altogether, this yields a constraint on the true stellar obliquity of $55^{+20}_{-18} \text{ deg}$ (Figure 3), which corroborates the likelihood of a misaligned Kepler-1656 b.

3. DISCUSSION

3.1. Dynamics in the Kepler-1656 system

As a consequence of Kepler-1656 b’s central transit and the uncertainty in $v \sin i_*$, our RM dataset is consistent with an aligned orbit but cannot rule out a misaligned λ as high as 57 deg at 2σ confidence. Of the other known exoplanets in the HEM track, only TOI-3362 b and HD 80606 b have obliquity measurements. The former is aligned, with $\lambda = 1.2 \pm 2.8 \text{ deg}$ (Espinoza-Retamal et al. 2023). Like Kepler-1656 b, TOI-3362 b orbits a single star, though it is not known if an outer giant planet exists in that system. HD 80606 b, on the other hand, is in a binary-star system and is misaligned, with $\lambda = 42 \pm 8 \text{ deg}$ (Pont et al. 2009; Hébrard, G. et al. 2010). Here we revisit plausible dynamics between Kepler-1656 b and c and their implications on b’s obliquity.

The simulations conducted by Angelo et al. (2022) that were most consistent with Kepler-1656 b and c’s orbital eccentricities and semimajor axes tended towards large mutual inclinations (60 deg–130 deg). The highly inclined companion excited e_b either to the point of tidal migration or maintained long-lasting ($>$ the age of the system) eccentricity oscillations. In either case, the inner planet’s obliquity tended towards misalignment; only $\sim 10\%$ of simulations yielded $\psi_b < 20 \text{ deg}$. In the long-lasting eccentricity oscillation scenario, $\sim 75\%$ of simulations produced $\psi_b > 60 \text{ deg}$. Simulations that migrated planet b into a tidally locked orbit were more consistent with alignment, though only $\sim 1/3$ rd had $\psi_b < 60 \text{ deg}$.

In the low-mutual-inclination regime, an eccentric ($e_c > 0.2$ –0.5) outer companion can still excite the inner planet’s eccentricity to large values ($\gtrsim 0.9$), in some cases causing the inner planet’s orbit to flip 180 deg from prograde to retrograde (Naoz et al. 2013; Li et al. 2014). If the eccentricity grows sufficiently large such that the periastron distance is small enough for strong tidal dissipation, the planet’s orbit will shrink and circularize. Petrovich (2015a) showed that throughout this coplanar HEM (CHEM), the migrating inner planet maintains a low stellar obliquity ($\psi < 30 \text{ deg}$) so long as the mutual inclination between the two planets is low ($\lesssim 20 \text{ deg}$).

Petrovich (2015a) derived the initial criteria for CHEM to operate: either (i) the inner planet begins in a circular orbit, in which case the outer planet must have $e_c \gtrsim 0.67$ and $M_b/M_c(a_b/a_c)^{1/2} \lesssim 0.3$, or (ii) both planets begin eccentric ($e \gtrsim 0.5$) and $M_b/M_c(a_b/a_c)^{1/2} \lesssim 0.16$. Given the posterior distributions in mass and semimajor axis for both planets (Angelo et al. 2022), this ratio for Kepler-1656 is $M_b/M_c(a_b/a_c)^{1/2} = 0.11 \pm 0.02$,

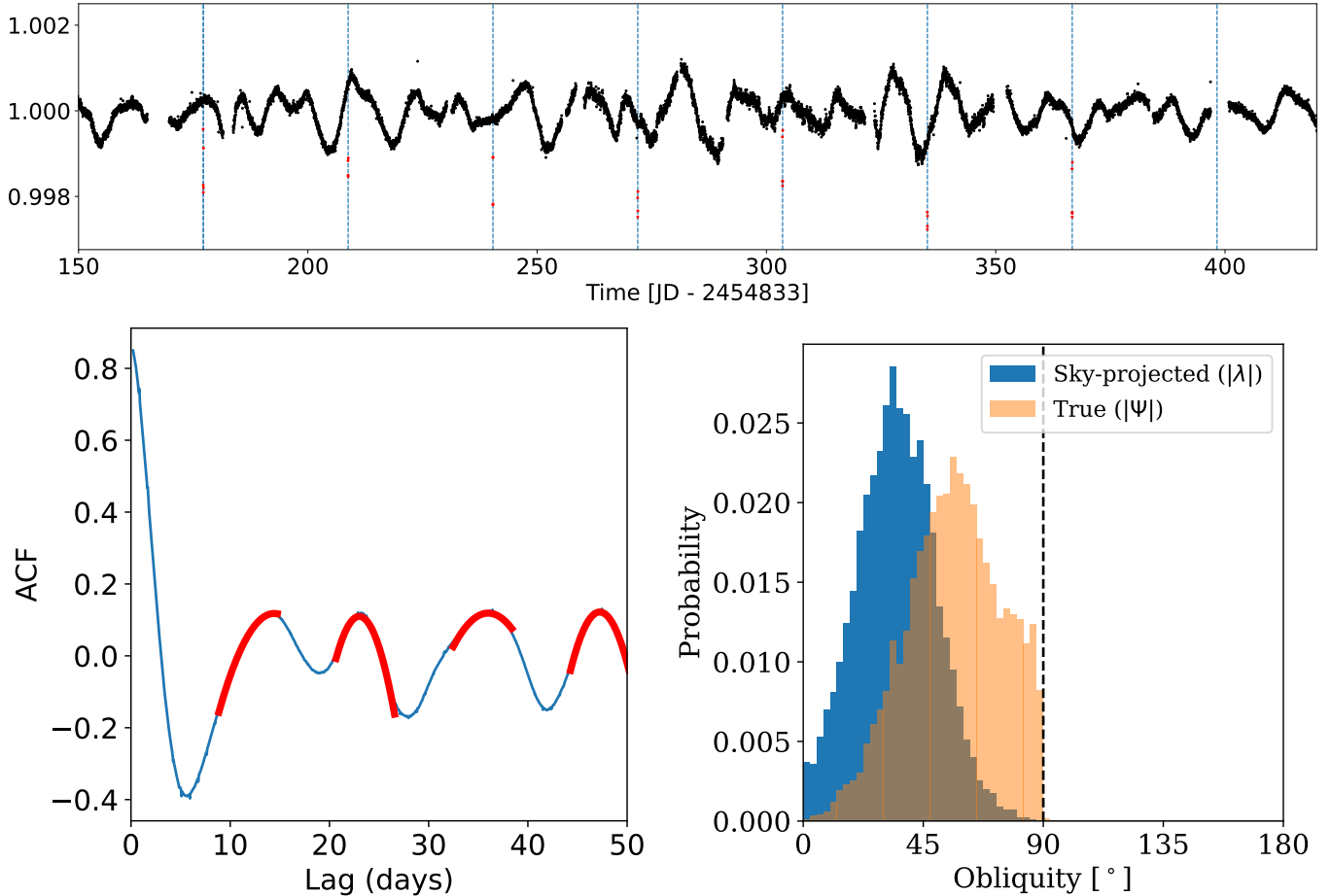


Figure 3. **Top:** Representative snippet of the *Kepler* photometry. Transit windows are highlighted by the vertical blue bands, with in-transit data marked in red. **Lower left:** Autocorrelation function of the full *Kepler* photometry using `spinspotter`. **Lower right:** Corresponding true obliquity distribution (orange) given the measured sky-projected obliquity (blue).

and is less than 0.16 at 99.2% confidence. This calculation assumed $M_c \sin i_{\text{orb},c}$ in place of M_c , i.e., the planets are coplanar. The true mass of Kepler-1656 c may be larger, in which case this ratio would be smaller, still satisfying the CHEM criterion. Thus, given Kepler-1656 c’s presently measured eccentricity (0.53 ± 0.05 ; Angelo et al. 2022), CHEM is a plausible explanation if either Kepler-1656 b formed with—or was able to gain—an eccentricity > 0.5 , or if Kepler-1656 c used to be moderately more eccentric ($\gtrsim 0.67$). Such eccentricities are naturally produced by planet-planet scattering events (e.g., Chatterjee et al. 2008).

We integrated the three-body equations of motion expanded to octupole order (Ford et al. 2000) as described in the appendix of Petrovich (2015b), given the measured planet masses of Angelo et al. (2022). We initialized planet b with an eccentricity of 0.2 at semimajor axis 0.5 AU and planet c with an eccentricity of 0.67 at its present-day semimajor axis of 3 AU. We included tidal dissipation in planet b parameterized with a 0.01 yr

viscous timescale² and Love number 0.25. We ran three simulations with the inner planet aligned at 0 deg obliquity but with the outer planet at 5 deg, 10 deg, and 15 deg mutual inclination. We found in all three cases the inner planet’s eccentricity became excited up to 0.94 and underwent oscillations for ~ 100 Myr before tidal effects quenched oscillations and triggered planet b’s migration into a HJ-like orbit. We stress that while the migration phase of the simulation agrees with the data, it is relatively short-lived (< 100 Myr) and thus has a low probability of being observed. We conclude that CHEM could be operating in the Kepler-1656 system, but the data remain consistent with a non-migrating in-situ formed planet b being observed at a snapshot

² For simplicity, we have adopted a much lower viscous timescale than Angelo et al. (2022) of 1.5 yr, allowing significant migration within $\sim 10^8$ yr. For reference, a viscous timescale of 0.01 yr (1.5 yr) is equivalent to setting a tidal quality factor of $Q_b \sim 10^4$ ($Q_b \sim 10^6$) at the planet’s current location.

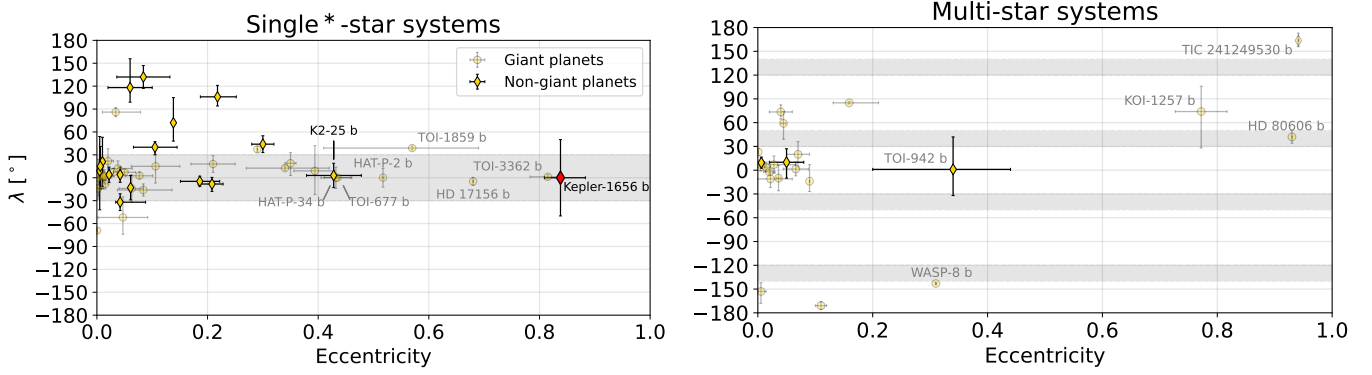


Figure 4. Projected obliquity λ for measured systems as a function of eccentricity, for single-star systems (left) and multi-star systems. The shaded bar on the left plot covers ± 20 deg, the range of obliquities for which CHEM could operate given an appropriate companion with zero stellar obliquity. The shaded bands on the multi-star plot highlight ± 10 deg and ± 130 deg corresponding to the bimodal peaks of the expected true obliquity distribution from star-planet Kozai (Anderson et al. 2016). Note that these angles refer to the true orbital inclinations, while the data points are for λ , the sky projection. The true obliquity ψ is between λ and $\text{sign}(\lambda)90$ deg. The data are the same from Figure 1, supplemented with updates for HD 80606 b (42 ± 8 deg; Hébrard, G. et al. 2010) and 55 Cnc e (11_{-20}^{+17} deg Zhao et al. 2023), and the addition of TIC 241249530 b ($163.5_{-7.7}^{+9.4}$ deg Gupta et al. 2024), TOI-3362 b (1.2 ± 2.8 deg; Espinoza-Retamal et al. 2023), TOI 677 b (0.3 ± 1.3 deg; Sedaghati et al. 2023; Hu et al. 2024), and of course Kepler-1656 b, where we have drawn the 1σ upper-limit of 50deg (this work).

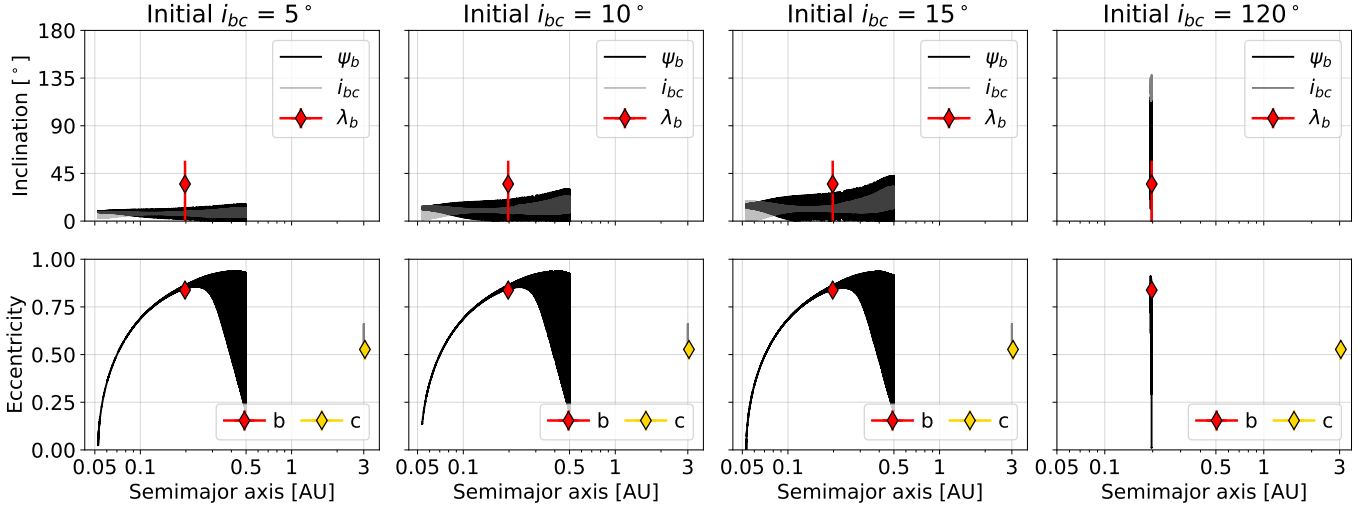


Figure 5. Three-body simulations of the orbits of Kepler-1656 b (black) and c (grey), for variable initial mutual inclinations i_{bc} , (5 deg, 10 deg, 15 deg, and 120 deg from left to right). The top row shows the evolution of the mutual inclination (grey) and the inner planet's obliquity (black), as a function of semimajor axis. The lower panel shows the eccentricity evolution of planet b (black) and c (grey). The first three ($i_{bc} \leq 15$ deg) are initialized as described in Section 3.1. The fourth ($i_{bc} = 120$ deg) is an example of a simulation from Angelo et al. (2022) initialized *in-situ* with a circular planet b. All four scenarios can reproduce the observed Kepler-1656 system (red and yellow data points). Though, $i_{bc} \leq 15$ deg requires starting planet b at a more distant orbit that subsequently migrates through its present-day location, before circularizing in ~ 100 Myr; larger mutual inclinations excite large eccentricities without triggering migration, with brief excursions to low obliquity over many \sim Gyr. The measured projected obliquity is plotted for the positive- λ scenario (to match $\psi_b > 0$) in the top panel at 35 deg with errorbars covering 0 deg–50 deg.

of high-eccentricity oscillations, as suggested by [Angelo et al. \(2022\)](#). The key to distinguishing these scenarios is the planet-perturber mutual inclination. Unfortunately, at 186 ± 0.5 pc ([Gaia Collaboration et al. 2023](#)) Kepler-1656 (V=11.6) is too far for such a measurement with Gaia astrometry. The expected astrometric signal from Kepler-1656 c is just $5.2 \mu\text{as}$, but at $G = 11$ we can expect a single-epoch precision of $34.2 \mu\text{as}$ with Gaia ([Perryman et al. 2014](#)).

3.2. Kepler-1656 in context

[Espinoza-Retamal et al. \(2023\)](#) noted a dichotomy in eccentric ($e \gtrsim 0.3$) planet obliquities; those in single-star³ systems tend to be aligned, while those in multi-star systems tend to be misaligned. We plot the updated λ - e diagram in Figure 4. For single-star systems, the next most eccentric sub-Saturn ($< 100 M_{\oplus}$) with a measured obliquity is K2-25 b ($e = 0.43 \pm 0.05$, $\lambda = 3.0 \pm 16.0$ deg; [Stefansson et al. 2020](#)). Kepler-1656 b and HAT-P-2 b ([de Beurs et al. 2023](#)), a HJ, are the only highly eccentric ($e > 0.3$) exoplanets with fully measured outer planetary companions.

If close-in exoplanets, large and small alike, form primarily from HEM, Figure 4 suggests that the identity of the perturber plays the key role in determining the obliquity. In multi-star systems, exoplanets with large obliquities span a wide range of mutual inclinations with their outer stellar companions ([Behmard et al. 2022](#); [Rice et al. 2024](#)). Though, there is an overabundance of edge-on binary orbits for systems hosting transiting exoplanets compared to field binaries, suggestive of a tendency towards mutual alignment ([Dupuy et al. 2022](#); [Rice et al. 2024](#)). It is still a small sample size, but the four oblique and eccentric exoplanets in multi-star systems (see Figure 4) have obliquities near those expected from star-planet Kozai (e.g. [Anderson et al. 2016](#)), which requires mutual inclinations > 39.2 deg ([Kozai 1962](#); [Lidov 1962](#); [Naoz 2016](#)). [Rice et al. \(2024\)](#) calculated the “linear motion parameter” (γ ; [Tokovinin & Kiyaveva 2015](#)), for WASP-8 B (4.0 ± 0.5 deg) and HD 80606 B (174.3 ± 0.3 deg). Both are consistent with edge-on orbits and perhaps mutual alignment, which in addition to the wide separation for HD 80606 B would make Kozai less likely. KOI-1257 is unresolved by *Gaia*, preventing an astrometric detection. However, computing γ for TIC 241249530 from its *Gaia* DR3 astrometry ([Gaia Collaboration et al. 2023](#)) yields 85.9 ± 36.0 deg, which could indicate a near face-on orbit and thus a significant mu-

tual misalignment. Interpreting inclinations from the γ parameter alone is still poorly constrained and degenerate with eccentricity. Longer baseline multi-epoch astrometry is needed to constrain individual systems.

Exoplanets in single-star systems, by definition, must instead be perturbed by outer planetary companions. Cold Jupiter companions in systems with inner small exoplanets show a tendency towards coplanarity ([Masuda et al. 2020](#)). This would preclude classical Kozai oscillations, though eccentric coplanar outer companions could still excite large eccentricities via the EKL mechanism ([Naoz 2016](#)). In such systems, CHEM could produce close-in but aligned planets. On the other hand, large mutual inclinations have been observed in the π Men and HAT-P-11 systems. Both have large (polar) mutual inclinations between inner and outer planet (as evidenced by *Gaia* astrometry; [Xuan & Wyatt 2020](#)). In such systems, ongoing nodal precession will make it more likely than not to observe the planet in a misaligned orbit ([Becker et al. 2017](#)). Accordingly, π Men c is slightly misaligned ($\psi = 26.9^{+5.8}_{-4.7}$ deg; [Kunovac Hodžić et al. 2021](#)) and HAT-P-11 b is near-polar ($\lambda = 106^{+15}_{-12}$ deg; [Winn et al. 2010](#); [Sanchis-Ojeda & Winn 2011](#)). So while there may not be a mutual inclination requirement for exciting eccentricities, and consequently triggering migration, the obliquity of the inner planet is likely still dependent. For the closest systems (< 60 – 100 pc), the full astrometric timeseries in the upcoming *Gaia* DR4 will enable constraints on the outer planet’s inclination ([Espinoza-Retamal et al. 2023](#)).

4. CONCLUSIONS

We measured the stellar obliquity of Kepler-1656 b from the Rossiter-McLaughlin anomaly observed with the Keck Planet Finder. We found the orbit to be consistent with alignment, but could not rule out misalignments up to 57 deg at 2σ confidence. Kepler-1656 b is one of four exoplanets to have an obliquity measurement that lives in the HEM track of the $e - a$ diagram. Two of these are in multi-star systems and are misaligned, while TOI-3362 b orbits a single star and is aligned. The mutual inclination of the perturber likely plays a leading role in determining the migration process and subsequently the obliquity of the migrating/migrated planet.

Since obliquity damping is less efficient for small planets ($\tau_{\psi} \propto (M_p/M_*)^{-2}$; [Hut 1981](#)), the obliquity distribution of small planets offers a more pristine view of post-migration obliquities, analogous to HJs around hot stars. There is a growing population within the $< 100 M_{\oplus}$ regime of polar orbits ([Attia et al. 2023](#)) which has been noted for the HJs ([Albrecht et al. 2022b](#)) but is not yet statistically robust in that sample ([Dong](#)

³ *The presence of stellar companions is not homogeneously constrained. For simplicity, here we define “single star” to be those in the Exoplanet Archive with `sy_snum==1`.

& Foreman-Mackey 2023; Siegel et al. 2023). Kepler-1656 b represents a rare example of such a proto-hot-Neptune/Saturn that could be in the act of migrating, kick-started by its outer planetary companion. If obliquities are not excited in conjunction with HEM, then post-migration dynamics must be important for exciting the broad obliquity distribution we observe today.

5. ACKNOWLEDGEMENTS

Some of the data presented herein were obtained at Keck Observatory, which is a private 501(c)3 non-profit organization operated as a scientific partnership among the California Institute of Technology, the University of California, and the National Aeronautics and Space Administration. The Observatory was made possible by the generous financial support of the W. M. Keck Foundation. Keck Observatory occupies the summit of Maunakea, a place of significant ecological, cultural, and spiritual importance within the indigenous Hawaiian community. We understand and embrace our accountability to Maunakea and the indigenous Hawaiian community, and commit to our role in long-term mutual stewardship. We are most fortunate to have the opportunity to conduct observations from Maunakea.

R.A.R. acknowledges support from the National Science Foundation through the Graduate Research Fellow-

ship Program (DGE 1745301). A.W.H. acknowledges funding support from NASA award 80NSSC24K0161 and the JPL President’s and Director’s Research and Develop Fund. CP acknowledges support from ANID BASAL project FB210003, FONDECYT Regular grant 1210425, CASSACA grant CCJRF2105, and ANID+REC Convocatoria Nacional subvencion a la instalacion en la Academia convocatoria 2020 PAI77200076. D.H. acknowledges support from the Alfred P. Sloan Foundation, the National Aeronautics and Space Administration (80NSSC21K0652), and the Australian Research Council (FT200100871).

This research was carried out, in part, at the Jet Propulsion Laboratory and the California Institute of Technology under a contract with the National Aeronautics and Space Administration and funded through the President’s and Director’s Research & Development Fund Program.

Facility: Keck:I (KPF) (Gibson et al. 2020)

Software: `astropy` (Astropy Collaboration et al. 2022), `corner` (Foreman-Mackey 2016), `emcee` (Foreman-Mackey et al. 2013), `matplotlib` (Hunter 2007), `numpy` (Harris et al. 2020), `pandas` (pandas development team 2020), `PyDE` (Parviainen 2016), `rmfit` (Stefánsson et al. 2022), `scipy` (Virtanen et al. 2020), `spinspotter` (Holcomb et al. 2022),

REFERENCES

- Albrecht, S., Winn, J. N., Johnson, J. A., et al. 2012, *ApJ*, 757, 18
- Albrecht, S. H., Dawson, R. I., & Winn, J. N. 2022a, *PASP*, 134, 082001
- Albrecht, S. H., Marcussen, M. L., Winn, J., Dawson, R., & Knudstrup, E. 2022b, in *Bulletin of the American Astronomical Society*, Vol. 54, 501.05
- Anderson, K. R., Storch, N. I., & Lai, D. 2016, *MNRAS*, 456, 3671
- Angelo, I., Naoz, S., Petigura, E., et al. 2022, *AJ*, 163, 227
- Astropy Collaboration, Price-Whelan, A. M., Lim, P. L., et al. 2022, *ApJ*, 935, 167
- Attia, O., Bourrier, V., Delisle, J. B., & Eggenberger, P. 2023, *A&A*, 674, A120
- Baranne, A., Queloz, D., Mayor, M., et al. 1996, *A&AS*, 119, 373
- Becker, J. C., Vanderburg, A., Adams, F. C., Khain, T., & Bryan, M. 2017, *AJ*, 154, 230
- Behrard, A., Dai, F., & Howard, A. W. 2022, *The Astronomical Journal*, 163, 160.
<https://dx.doi.org/10.3847/1538-3881/ac53a7>
- Brady, M. T., Petigura, E. A., Knutson, H. A., et al. 2018, *AJ*, 156, 147
- Brewer, J. M., Fischer, D. A., Valenti, J. A., & Piskunov, N. 2016, *ApJS*, 225, 32
- Brown, T. M., Gilliland, R. L., Noyes, R. W., & Ramsey, L. W. 1991, *ApJ*, 368, 599
- Chaplin, W. J., Cegla, H. M., Watson, C. A., Davies, G. R., & Ball, W. H. 2019, *AJ*, 157, 163.
<https://dx.doi.org/10.3847/1538-3881/ab0c01>
- Chatterjee, S., Ford, E. B., Matsumura, S., & Rasio, F. A. 2008, *ApJ*, 686, 580
- Dawson, R. 2014, *Astrophysical Journal Letters*, 790, doi:10.1088/2041-8205/790/2/L31
- Dawson, R. I., & Johnson, J. A. 2018, *ARA&A*, 56, 175
- de Beurs, Z. L., de Wit, J., Venner, A., et al. 2023, *The Astronomical Journal*, 166, 136.
<https://dx.doi.org/10.3847/1538-3881/acedf1>
- Dong, J., & Foreman-Mackey, D. 2023, *AJ*, 166, 112
- Dong, J., Huang, C. X., Zhou, G., et al. 2021, *The Astrophysical Journal Letters*, 920, L16.
<https://dx.doi.org/10.3847/2041-8213/ac2600>

- Dupuy, T. J., Kraus, A. L., Kratter, K. M., et al. 2022, *MNRAS*, 512, 648
- Eastman, J., Gaudi, B. S., & Agol, E. 2013, *PASP*, 125, 83
- Espinoza-Retamal, J. I., Zhu, W., & Petrovich, C. 2023, *The Astronomical Journal*, 166, 231.
<https://dx.doi.org/10.3847/1538-3881/ad00b9>
- Espinoza-Retamal, J. I., Brahm, R., Petrovich, C., et al. 2023, *ApJL*, 958, L20
- Fabrycky, D., & Tremaine, S. 2007, *ApJ*, 669, 1298
- Ford, E. B., Kozinsky, B., & Rasio, F. A. 2000, *The Astrophysical Journal*, 535, 385.
<https://dx.doi.org/10.1086/308815>
- Foreman-Mackey, D. 2016, *JOSS*, 1
- Foreman-Mackey, D., Hogg, D. W., Lang, D., & Goodman, J. 2013, *PASP*, 125, 306
- Gaia Collaboration, Vallenari, A., Brown, A. G. A., et al. 2023, *A&A*, 674, A1
- Gelman, A., Carlin, J. B., Stern, H. S., & Rubin, D. B. 2003, *Bayesian Data Analysis*, 2nd edn. (Chapman and Hall)
- Gibson, S. R., Howard, A. W., Marcy, G. W., et al. 2016, in *Society of Photo-Optical Instrumentation Engineers (SPIE) Conference Series*, Vol. 9908, *Ground-based and Airborne Instrumentation for Astronomy VI*, ed. C. J. Evans, L. Simard, & H. Takami, 990870
- Gibson, S. R., Howard, A. W., Roy, A., et al. 2018, in *Society of Photo-Optical Instrumentation Engineers (SPIE) Conference Series*, Vol. 10702, *Ground-based and Airborne Instrumentation for Astronomy VII*, ed. C. J. Evans, L. Simard, & H. Takami, 107025X
- Gibson, S. R., Howard, A. W., Rider, K., et al. 2020, in *Society of Photo-Optical Instrumentation Engineers (SPIE) Conference Series*, Vol. 11447, *Society of Photo-Optical Instrumentation Engineers (SPIE) Conference Series*, 1144742
- Gupta, A. F., Millholland, S. C., Im, H., et al. 2024, *Nature*, doi:10.1038/s41586-024-07688-3.
<https://doi.org/10.1038/s41586-024-07688-3>
- Harris, C. R., Millman, K. J., van der Walt, S. J., et al. 2020, *Nature*, 585, 357–362
- Hébrard, G., Désert, J.-M., Díaz, R. F., et al. 2010, *Å*, 516, A95. <https://doi.org/10.1051/0004-6361/201014327>
- Hirano, T., Suto, Y., Winn, J. N., et al. 2011, *ApJ*, 742, 69
- Hogg, D. W., & Foreman-Mackey, D. 2018, *The Astrophysical Journal Supplement Series*, 236, 11.
<https://dx.doi.org/10.3847/1538-4365/aab76e>
- Holcomb, R. J., Robertson, P., Hartigan, P., Oelkers, R. J., & Robinson, C. 2022, *The Astrophysical Journal*, 936, 138. <https://dx.doi.org/10.3847/1538-4357/ac8990>
- Hu, Q., Rice, M., Wang, X.-Y., et al. 2024, *AJ*, 167, 175
- Hunter, J. D. 2007, *CSE*, 9, 90
- Hut, P. 1981, *A&A*, 99, 126
- Ito, T., & Ohtsuka, K. 2019, *Monographs on Environment, Earth and Planets*, 7, 1
- Kozai, Y. 1962, *AJ*, 67, 591
- Kraft, R. P. 1967, *ApJ*, 150, 551
- Kunovac Hodžić, V., Triaud, A. H. M. J., Cegla, H. M., Chaplin, W. J., & Davies, G. R. 2021, *MNRAS*, doi:10.1093/mnras/stab237, stab237
- Lai, D. 2012, *MNRAS*, 423, 486
- Li, G., Naoz, S., Kocsis, B., & Loeb, A. 2014, *ApJ*, 785, 116
- Lidov, M. 1962, *Planet. Space Sci.*, 9, 719
- Masuda, K., Petigura, E. A., & Hall, O. J. 2022, *MNRAS*, 510, 5623
- Masuda, K., & Winn, J. N. 2020, *AJ*, 159, 81
- Masuda, K., Winn, J. N., & Kawahara, H. 2020, *AJ*, 159, 38
- McLaughlin, D. B. 1924, *ApJ*, 60, 22
- Naoz, S. 2016, *ARA&A*, 54, 441
- Naoz, S., Farr, W. M., Lithwick, Y., Rasio, F. A., & Teyssandier, J. 2011, *Nature*, 473, 187
- Naoz, S., Farr, W. M., Lithwick, Y., Rasio, F. A., & Teyssandier, J. 2013, *Monthly Notices of the Royal Astronomical Society*, 431, 2155.
<https://doi.org/10.1093/mnras/stt302>
- Naoz, S., Kocsis, B., Loeb, A., & Yunes, N. 2013, *ApJ*, 773, 187
- NASA Exoplanet Archive. 2019, *Confirmed Planets Table*, IPAC, doi:10.26133/NEA1. <https://catcopy.ipac.caltech.edu/doi/doi.php?id=10.26133/NEA1>
- pandas development team, T. 2020, *pandas-dev/pandas: Pandas, vlatest*, Zenodo, doi:10.5281/zenodo.3509134.
<https://doi.org/10.5281/zenodo.3509134>
- Parviainen, H. 2016, *PyDE: v1.5, vv1.5*, Zenodo, doi:10.5281/zenodo.45602.
<https://doi.org/10.5281/zenodo.45602>
- Pepe, F., Mayor, M., Galland, F., et al. 2002, *A&A*, 388, 632
- Perryman, M., Hartman, J., Bakos, G. Á., & Lindegren, L. 2014, *ApJ*, 797, 14
- Petigura, E. A. 2015, PhD thesis, University of California, Berkeley
- Petigura, E. A., Howard, A. W., Marcy, G. W., et al. 2017, *The Astronomical Journal*, 154, 107.
<https://dx.doi.org/10.3847/1538-3881/aa80de>
- Petrovich, C. 2015a, *ApJ*, 805, 75
- . 2015b, *ApJ*, 799, 27
- Petrovich, C., Muñoz, D. J., Kratter, K. M., & Malhotra, R. 2020, *ApJL*, 902, L5
- Piaulet, C., Benneke, B., Rubenzahl, R. A., et al. 2021, *AJ*, 161, 70

- Pont, F., Hébrard, G., Irwin, J. M., et al. 2009, *A&A*, 502, 695
- Rasio, F. A., & Ford, E. B. 1996, *Science*, 274, 954
- Rice, M., Gerbig, K., & Vanderburg, A. 2024, *AJ*, 167, 126
- Rice, M., Wang, S., & Laughlin, G. 2022, *ApJL*, 926, L17
- Rossiter, R. A. 1924, *ApJ*, 60, 15
- Rubenzahl, R. A., Dai, F., Howard, A. W., et al. 2021, *AJ*, 161, 119
- Sanchis-Ojeda, R., & Winn, J. N. 2011, *ApJ*, 743, 61
- Schlaufman, K. C. 2010, *ApJ*, 719, 602
- Sedaghati, E., Jordán, A., Brahm, R., et al. 2023, *AJ*, 166, 130
- Shporer, A., & Brown, T. 2011, *ApJ*, 733, 30
- Siegel, J. C., Winn, J. N., & Albrecht, S. H. 2023, *ApJL*, 950, L2
- Socrates, A., Katz, B., Dong, S., & Tremaine, S. 2012, *ApJ*, 750, 106
- Stefansson, G., Mahadevan, S., Maney, M., et al. 2020, *AJ*, 160, 192
- Stefansson, G., Mahadevan, S., Petrovich, C., et al. 2022, *ApJL*, 931, L15
- Teyssandier, J., Naoz, S., Lizarraga, I., & Rasio, F. A. 2013, *ApJ*, 779, 166
- Tokovinin, A., & Kiyeva, O. 2015, *Monthly Notices of the Royal Astronomical Society*, 456, 2070.
<https://doi.org/10.1093/mnras/stv2825>
- Virtanen, P., Gommers, R., Oliphant, T. E., et al. 2020, *NatMe*, 17, 261
- Winn, J. N., Fabrycky, D., Albrecht, S., & Johnson, J. A. 2010, *ApJL*, 718, L145
- Winn, J. N., Johnson, J. A., Howard, A. W., et al. 2010, *ApJL*, 723, L223
- Wu, Y. 2018, *AJ*, 155, 118
- Xuan, J. W., & Wyatt, M. C. 2020, *MNRAS*, 497, 2096
- Yee, S. W., Petigura, E. A., Fulton, B. J., et al. 2018, *AJ*, 155, 255
- Zanazzi, J. J., Dewberry, J., & Chiang, E. 2024, *arXiv e-prints*, arXiv:2403.05616
- Zhao, L. L., Kunovac, V., Brewer, J. M., et al. 2023, *Nature Astronomy*, 7, 198